Contents lists available at ScienceDirect

Arabian Journal of Chemistry

journal homepage: www.ksu.edu.sa

Original article

Investigation on structural, optical and anti-bacterial properties of organic additives iron oxide prepared by chemical route method

Talat Zeeshan [a], Asma Obaid [a], Salma Waseem [a], Muhammad Danish Ali [b,*], Zohra Kayani [a], Ameni Brahmia [c]

[a] Department of Physics, Lahore College for Women University, Lahore, Pakistan
[b] Institute of Physics, Centre for Science and Education, Silesian University of Technology, Krasinskiego 8A, 40-019, Katowice, Poland. Ph.D. School, Silesian University of Technology, 2a Akademicka Str., 44-100, Gliwice, Poland
[c] Department of Chemistry, College of Science, King Khalid University, 61413 Abha, Saudi Arabia

ARTICLE INFO

Keywords:
Antibacterial activity
XRD
Optical properties
Structural properties
Iron oxide

ABSTRACT

Technology and Nanoscience have a remarkable impact on environmental challenges. Scientists are moving away from harmful chemical approach and toward eco-friendly, accessible, efficient, and affordable green chemical methods for synthesizing nanoparticles. This article provides a feasible way to make iron oxide using an Avicennia marina dry fruit, seeds, leaves and green fruit extract. Structural, optical and morphological properties of the manufactured iron oxide nanoparticles have been evaluated using X-ray diffraction spectroscopy (XRD,) Ultra violet visible spectroscopy (UV–Visible), Fourier transform infrared spectroscopy (FT-IR), scanning electron microscope spectroscopy (SEM) and antibacterial activity. The formation of FeO NPs and their crystallinity has been confirmed by XRD, average particle size of FeO NP of dry fruit, seeds, leaves and green fruit are 7.1335 nm, 9.295 nm, 9.680 nm and 10.128 nm respectively. FT-IR spectrum shows the surface functionalization and vibrational phases of the bonds in FeO NPs. Band gap energies decreasing as crystallite size increases, according to UV visible results band gap energies of dry fruit, seeds, leaves and green fruit are 3.16 eV, 2.57 eV, 2.99 eV and 2.52 eV respectively. The antibacterial properties of the produced nanoparticles against Xanthomonas campestris pv vesicatoria, Erwinia spp, Escherichia coli bacteria has been investigated. Iron oxide nano particles has been utilized for antibacterial activity because of their less toxicity, high stability and biocompatibilities. The result shows the produced FeO NPs were minimize on bacterial colony.

1. Introduction

As an innovative discipline, a green technique to synthesizing nanoparticles has been developed. Nanoscience and technology have a huge impact on environmental challenges. The study of materials with one or more dimensions in the range of 1–100 nm is referred to as Nano science. Because, of the surface to volume ratio, nanomaterial have unique structural and physico-chemical characteristics when compared to bulk counterparts (Darroudi, 2014). These materials are created by the organizing of atoms and molecules or by the annihilation of a macroscopic material. Nanomaterials production technique is gaining popularity these days, owing to their broad use in a wide range of industries (Jayapriya et al., 2019). Nanoparticles (NPs) are particularly noteworthy among nanomaterials because of their ability to act as a link between macroscopic and atomic structures. Materials at the macroscopic level show a consistent pattern of behavior. Regardless of their size or mass, they all have the same qualities. Nanoparticles are currently being employed in numerous high-tech industries, such as the medical sector for diagnostics, antibacterial applications, and medication delivery systems, because of their distinct and unique features (Gholami, 2018; parveen et al., 2012). Nanoparticle research fills the gap between bulk materials and atomic-scale materials. Nanoparticles are made in a variety of ways and using a range of precursors. Recently Nanoparticles of iron, nickel, zinc, copper, silver, and gold are common because of their uses and incredible benefits (Amutha et al., 2019). Indeed, iron oxide nanoparticles (FeO-NPs) are particularly intriguing in modern nanotechnology research due to their distinct characteristics making them suitable for a variety of applications (Teja and Koh, 2009;

Peer review under responsibility of King Saud University.

* Corresponding author.
E-mail addresses: muali@polsl.pl, Danishmsc15@gmail.com (M. Danish Ali).

https://doi.org/10.1016/j.arabjc.2023.105581
Received 18 June 2023; Accepted 20 December 2023
Available online 23 December 2023

Laurent et al., 2008).

Biosynthesis of NPs is currently recognized as an environmentally beneficial strategy as no hazardous substance is used in bio-inspired procedures (Remya et al., 2017; Igwe and Nwamezie, 2018; Awwad et al., 2020).Plants have huge compositions of secondary metabolites and seem to be nature's "chemical factories." This could be used as a redox mediator as well as NP stabilizer. It has been observed that NPs synthesized utilizing plant extracts are much stable and have a faster rate of fabrication than those synthesized using conventional methods, because green approaches are environmentally friendly, economical, convenient, and easy to perform, and also no toxic agent has been used. Metal and metal oxide NPs were effectively synthesized via the green technology, and indeed the NPs have been used in a variety of applications.

Various chemical processes, such as sol–gel transition, supercritical fluid synthesis and pyrolysis are often used in the formation of nanoparticles. Engraving, thermal decomposition, mechanical milling, lithography and ablation laser are some of the physical processes used to deposit chemically in the steam phase (Rajivgandhi et al., 2020).These techniques are costly and need the use of harmful solvents (Ahila et al., 2018). On either hand, there has lately been a lot of work put into using ecologically benign ways to produce noble metal nanoparticles (Toropov, 2019).Green technologies, which attempt to generate very pure nanoparticles using simple, cost-effective, and repeatable procedures, have resulted from this endeavor. Plant or fruit extracts are mostly used to accomplish this it is seems that green method is low cost, quick and efficient, and generally in the development of crystalline nanoparticles in a variety of forms (leaves, stems, prisms, needles or plates) come in a variety of shapes and sizes.

Green synthesized and characterized iron oxide nanoparticles were evaluated for antibacterial properties. Because of their biocompatibility, iron oxide compounds are commonly used in biomedical methods (Nguyen, 2012). Many iron oxides are found naturally and may be fabricated in the lab. They are most often used in biomedical activities. Since this compound meet the requirements of (1) chemical stability in physiological conditions, (2) minimal toxicity, and (3) strong magnetic moments. Iron oxide nanoparticles shorter than 20 nm, like maghemite or magnetite, have distinctive characteristics. They have been used to separate and purify cell populations in biomedical applications such as diagnostic magnetic resonance imaging (MRI), medication administration to a cell or tissue, and cellular biology research (Tartaj and Morales, 2005), Because on the concentration and exposure time, the toxicity of iron oxide nanoparticles varies. At lower concentrations (10 mg/mL) and longer time of exposure (72 h), they are removed from the body. At large concentrations, they may cause oxidative cellular stress and affect responses such as DNA and gene expression. More research is still needed in this area (Patil et al., 2018).

Chemical, biological and physical processes are used to create iron oxide nanoparticles in the magnetite, maghemite, and hematite form (Attarad et al., 2016). Plants are one of the biological techniques for making iron oxide nanoparticles. Roots, seeds, fruits, and leaves are among the plant parts used. As a green approach to nanotechnology, phytochemicals play a key role in nanoparticle synthesis.

In a salty or brackish water environment, mangroves are found which are small trees or shrubs. In the tropical and sub-tropical zones, mangroves can be found in 118 countries. Mangroves are tall trees that can grow up to 25 m in height. Red, Black and white are three most common types among these seven. Black Mangroves are botanically known as Avicennia marina, and they are a thin, pale blackish grey colored shrub or tree that grows to a height of three to ten meters in saline environments. The extract's phytochemicals reduce and maintain the pH. **Karpagavinayagam, et al.** used an Avicennia marina flower extract to create iron oxide in a non-hazardous way. This greener promising work will aid in the development of the anti-toxicity, compatible in electrical & electronic industries and in getting better quality materials for life (Karpagavinayagam, 2019). **Velsankar, et al.** Celosia argentea leaf extract was used to efficiently biosynthesize iron oxide nanoparticles. the anti-inflammatory and anti-diabetic actions showed the highest activity, at 93 % and 87 %, respectively (RamalinVaikundamoorthy and Pandurangan Dhinesh, 2019). **Kanagasubbulakshmi, et al.** discovered that an untested Lagenaria siceraria leaf extract might be used for manufacturing iron oxide nanoparticles in an environmentally friendly manner. The synthesised FeO-NPs' antibacterial activity was assessed against Gram-positive and Gram-negative bacteria, including Escherchia coli and Staphylococcus aureus. Thus, a variety of biological applications can make use of naturally stabilized FeO-NPs with herbal properties (Kanagasubbulakshmi and Kadirvelu, 2017).

The current study has demonstrated the green route technique for producing iron oxide nanoparticles at a large scale, and it has also aided in the production of less costly nanoscale metal oxide particles with antibacterial properties. In this review, we mainly concentrate on the Avicennia marina dry fruit, seeds, leaves, and green fruit's biological synthesis of iron oxide nanoparticles. This study represents the first attempt on Avecinnia marina dry fruit, seeds, leaves, and green fruits to examine the FeO NPs, offering a valuable data and opening new avenues for research.

2. Experimentation

Since Avicennia marina is a widely dispersed mangrove plant, it is easily accessible and might be a reasonably priced option for producing FeO-NPs on a big scale. Because the natural extract doesn't produce any hazardous byproducts, it's a safer and more sustainable option (Krishnan et al., 2020).

The Avicennia marina's dry fruit, seeds, leaves and green fruit extract made by green method. The dry fruit seeds, leaves and green fruit were carefully washed multiple time with distilled water and dried for two weeks in the sun light after that milled to form a fine powder. 5 g of powder were weighted and added 100 mL of distilled water. The mixture was boiled until 15 min, subsequently cooled, then Whatman No. 1 filter paper was used to filter. 20 mL of Avicennia marina extract was added with 80 mL of aqueous ferric chloride solution (1 mmol) applied drop by drop with steady stirring for 2–3 h. To eliminate contaminants, the mixture was three times washed with distilled water after being centrifuged at 10,000 rpm for 30 min. The mixture is held at 15psi pressure and 125 °C for 120 min in oven. When oxygen or other unknown matter is existing in the oven, it can alter the reaction; however, by employing a vacuum oven, such unwanted reactions can be avoided, and particles could be contaminant-free.

3. Anti-bacterial activity

For the anti-bacterial analysis, the laminar flow chamber and hand were sterilized in the ethyl alcohol to prevent contamination impact. Furthermore, the autoclave was used to sanitize petri plate dishes for 20 min at 121 °C. The plates were kept at room temperature for the entire night in order to look for signs of contamination. A sterile stainless steel cork borer was used to create 6 mm diameter agar wells. A saline suspension of isolated colonies that were chosen from nutrient agar plates and cultivated for 18 to 24 h was used to create the bacterial suspension. The medium was developed to isolate the microflora of LBA (Luria Bertani Agar). Luria Bertani Agar was created by diluting yeast extract (25 g), sodium chloride (2.5 g), agar (7.5 g) and tryptone (5 g) in distilled water. The aforementioned mixture was autoclave sterilized at 121 °C and 15 pressure for 20 min. LBA mediums were prepared after the media has been placed on petri dishes and allowed time to setup for the isolation and bacterial strain purification.

4. Results and discussion

X-ray diffractometer (XRD) of Germany model: D8-Discover with

Cukα of 1.5406 Å was used for study crystallographic of the samples. Scanning was performed in the range 2θ 10°- 80° with a scan speed of 2 per min. FTIR spectroscopy from MIDAC 2000, USA, was also used to confirm the structure. The JSM 7400F Scanning Electron Microscope (SEM) was used to examine the morphology. The UV–Visible spectroscopy model U-2800 spectrometer. ROM vers-250107 used to study the optical properties of synthesized FeO NPs.

4.1. X-ray diffraction

The diffracted pattern intensities of the powder specimen of FeO nano particles were studied to investigate the crystallographic nature of the nanoparticles as shown in Fig. 2.

The Fig. 1 shows the XRD analysis of iron-oxide nanoparticles obtained through green synthesis method using Avicennia marina dry fruit, seeds, leaves and green fruit extract exhibit the sharpness of peaks that indicate good crystallinity of the nanoparticles. The XRD data indicates the crystallographic planes of face centered cubic structure of FeO NPs are (220), (311), (222), (400),(422),(511),(440), (622). Visualized at 29°, 35.5°, 36.8°, 43°, 55°, 57°, 62.8°, 73°. The diffraction obtained at 2θ = 35° can be attributed to FeO NPs in accordance with JCPDS card No.19–0629. The most intense peak (311) recorded in the XRD analysis is fitted by the Gaussian fit to measure the crstallite size. (see Table 1). Using Scherrer's formula (A et al., 2007):

$$D = k\lambda/\beta\cos\theta \quad (4.1)$$

Where, k is the Scherer constant (0.94), λ is the x-ray wavelength (1.54 A°), β is the full width half maxima of corresponding peaks and θ is the Bragg's angle.

The crystallite size can be determined from the full width at half maximum intensity (FWHM) estimated on the intense diffracted peak (311). The crystallite size of iron oxide nanoparticles of Avicennia marina's (dry fruit, seeds leaves and green fruit) with crystallite size (7.1335 nm, 9.295 nm, 9.680 nm, 10.128 nm) respectively. It has been observed from the graph that crystallite size of green fruit is maximum (10.128 nm) whereas for dry fruit is minimum (7.113) nm. As a result of the structure contracting, the size of the nanoparticles decreases when tiny size atoms fill the spaces left by large - sized atoms. Fig. 3 demonstrates the magnified view of most intense peak at (311) which shift towards the higher 2θ value which is the confirmation of lowest crystallite size of green fruit.(See Fig. 4).

The lattice parameter of the prepared FeO NPs is estimated using the subsequent equation (C et al., 1978):

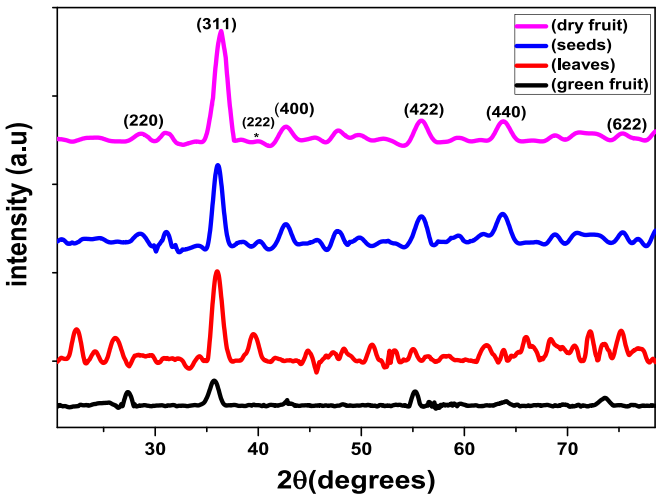

Fig. 2. X-ray Diffraction pattern of the synthesized FeO-NPs.

Table 1
Structural parameter extracted from XRD.

Sample	Position 2(θ) (Degree)	FWHM (Degree)	Lattice parameter (A°)	Crystallite size (nm)	Dislocation line density (lines/cm^2)
Dry fruit	35.27	1.1138	8.404	7.133	9.7474×10^{11}
Seeds	35.72	0.8547	9.228	9.295	1.9651×10^{12}
Leaves	36.99	0.8208	8.046	9.680	1.1573×10^{12}
Green fruit	35.08	0.7844	8.48	10.128	1.0672×10^{12}

$$a = \lambda/2\sin\theta\left[\left(h^2 + k^2 + l^2\right)\right]^{1/2} \quad (4.2)$$

The lattice parameter of dry fruit, seeds, leaves, and green fruit are 8.404A°, 9.228A°, 8.046A° and 8.48A° respectively. As the lattice parameter is influenced by the particle size, so the dry fruit has smaller particles are said to have a large surface area and high surface energy (Imanipour et al., 2020).

The distance between magnetic ions is studied as hopping length.

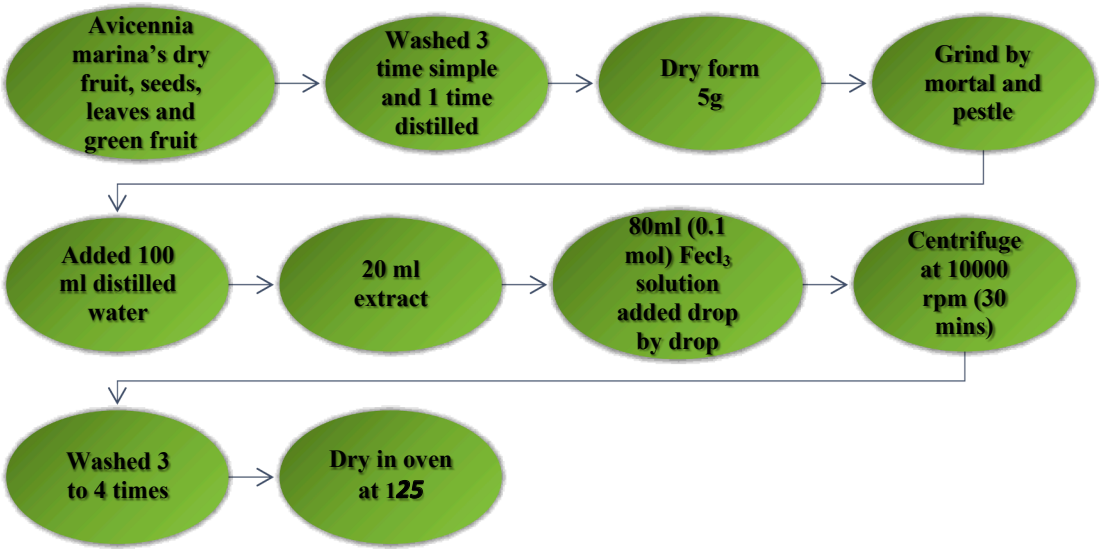

Fig. 1. Flowchart for synthesis of FeO NPs.

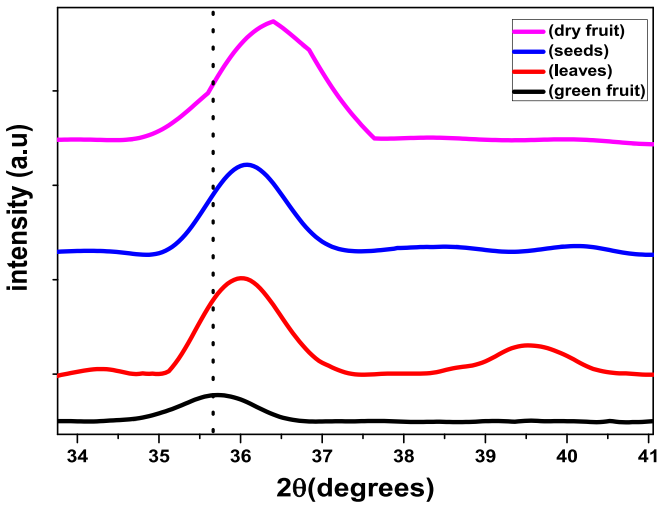

Fig. 3. Magnified view of peak (311).

The hopping length of A-side (L_A) and B-site (L_B) are measured by the formula in equations (Zeeshan et al., 2021):

$$L_A = a\left[\frac{\sqrt{3}}{4}\right] \tag{4.3}$$

$$L_B = a\left[\frac{\sqrt{2}}{4}\right] \tag{4.4}$$

It is well recognized that the hopping length is affected by the lattice parameter, accordingly the hopping length of seeds is maximum due to the lattice parameter of seed is highest.

The X-ray density of fabricated FeO NPs has been measured with the help of equation as follow (Nadi, 2013):

$$d_x = 8M/Na^3 \tag{4.5}$$

Where N ($6.0225x10^{23}$) is Avogadro's number, M is molecular weight of the sample, 8 is the number of unit cell and "a" is the lattice parameter. It has been illustrated through Fig. 5 that X-ray density of green fruit is maximum which may be due to the reduction in size. It is commonly identified that the distance among the individual atom decreases leads to the atoms in the material come close to each other that in turns reduce the X-ray density. Additionally, the dislocation density may drop at grain boundaries as a result of an expansion in crystallite size, which is caused by a reduction in dislocation density.

4.1.1. *Williamson-Hall plot*

This methodology is ascribed by G. K. Williamson and his student, W. H. Hall. It is founded on the idea that the approximations of the size-broadening equations βL, and strain broadening βc, diverge significantly with respect to Bragg angle θ, (Williamson and Hall, 1953).

The statistics on strain (ε) and crystallite size (D) of FeO NPs was calculated from β_{hkl} utilizing the Williamson-Hall relation. In the W-H approach, strain broadening is expressed as follows (Sen et al., 2020):

$$\beta s = 4\varepsilon tan\theta \tag{4.10}$$

The observed line's width is measured by adding the β_{strain} and β_D [51]:

$$\beta_{hkl} = \beta_{strain} + \beta_D \tag{4.11}$$

The resulting equation is;

$$\beta_{hkl} = \frac{k\lambda}{Dcos\theta} + 4\varepsilon tan\theta \tag{4.12}$$

Here K is the Scherrer constant which is 0.94 and ε is the internal strain. According to the W-H technique, the "strain" profile and the "crystallite size" profile both contributed to the line enlargement. In this methodology, the graph of β_{hkl} cosθ (y-axis) vs. 4sinθ (x-axis) illustrating

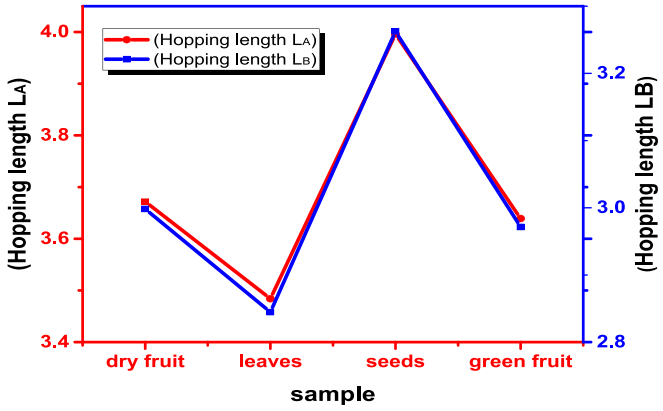

Fig. 5. Variation in hopping length LA and LB.

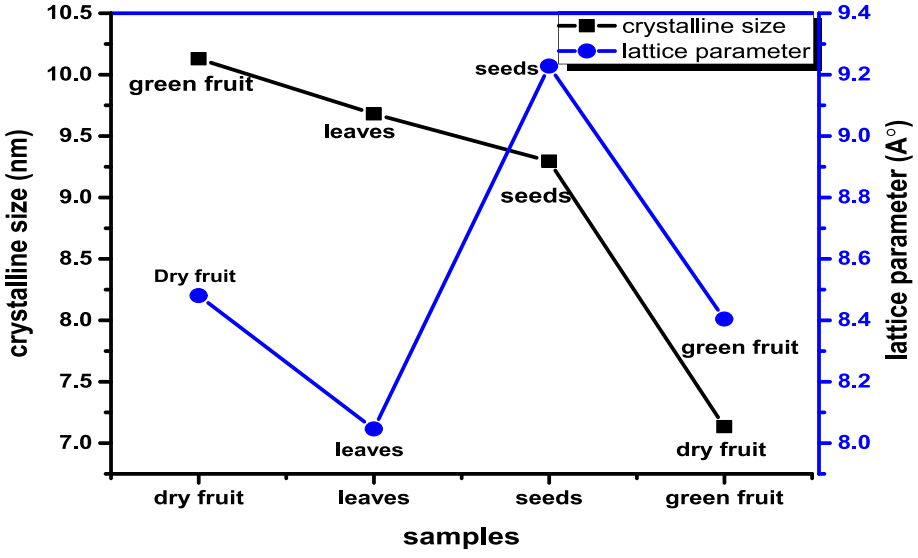

Fig. 4. Variation of crystallite size and lattice parameter for FeO NPs.

the intense peaks of FeO NPs shown in Fig. 6. The slope and intercept of linear fit data determine the amount of strain (ε) and crystalline size D_{W-H}, respectively.

It has been observed from the W-H plot the slope (lattice strain) is positive for green fruit, seeds and dry fruit and for leaves slop is negative. The positive slope value represents the tensile strain while the negative value of strain shows the presence of compressive strain. The observed positive strain results in an expansion of the crystal structure that may be due to lattice contraction. The crystallite size calculated by W-H plot has smaller values than Debye Scherrer method of green fruit, leaves and seeds while dry fruit has larger crystallite size. It has been observed from graph W-H plot crystallite size has same trend as Debye Scherrer crystallite size. The calculated values of crystallite size and strain of FeO NPs by W-H plot are summarized in Table 2.

Table 2
Crystallite size and lattice strain of the FeO NPs by Debye-Sherrer and Williamson Hall plot.

Samples	D-S and Williamson crystallite size (nm)		W-H Plot Lattice strain
Dry fruit	7.13352193	0.378484	0.34981
Seeds	9.29556632	0.386736	0.29533
Leaves	9.68004064	0.960008	−30.71277
Green fruit	10.1287405	15.46	0.00259

4.2. Fourier transforms infrared spectroscopy (FTIR)

The vibrational phases of the bonds in FeO-NPs used in Fourier transform infrared spectroscopy (FTIR) to understand more about the nano-particles (NPs) structure. The FTIR peaks of FeO nano particles were recognized in the range 400–4000 cm^{-1} shown in Fig. 7. **C–H stretching** causes the aromatic and aliphatic bands between 2350 cm^{-1}-2924 cm^{-1}, the enzymes in the plants cause these aliphatic and aromatic bonds to form. Metal-oxygen bond **(Fe-O)** is found in the range of 400–850 cm^{-1}. The extract's spectra display peaks at 3124 cm^{-1}, which

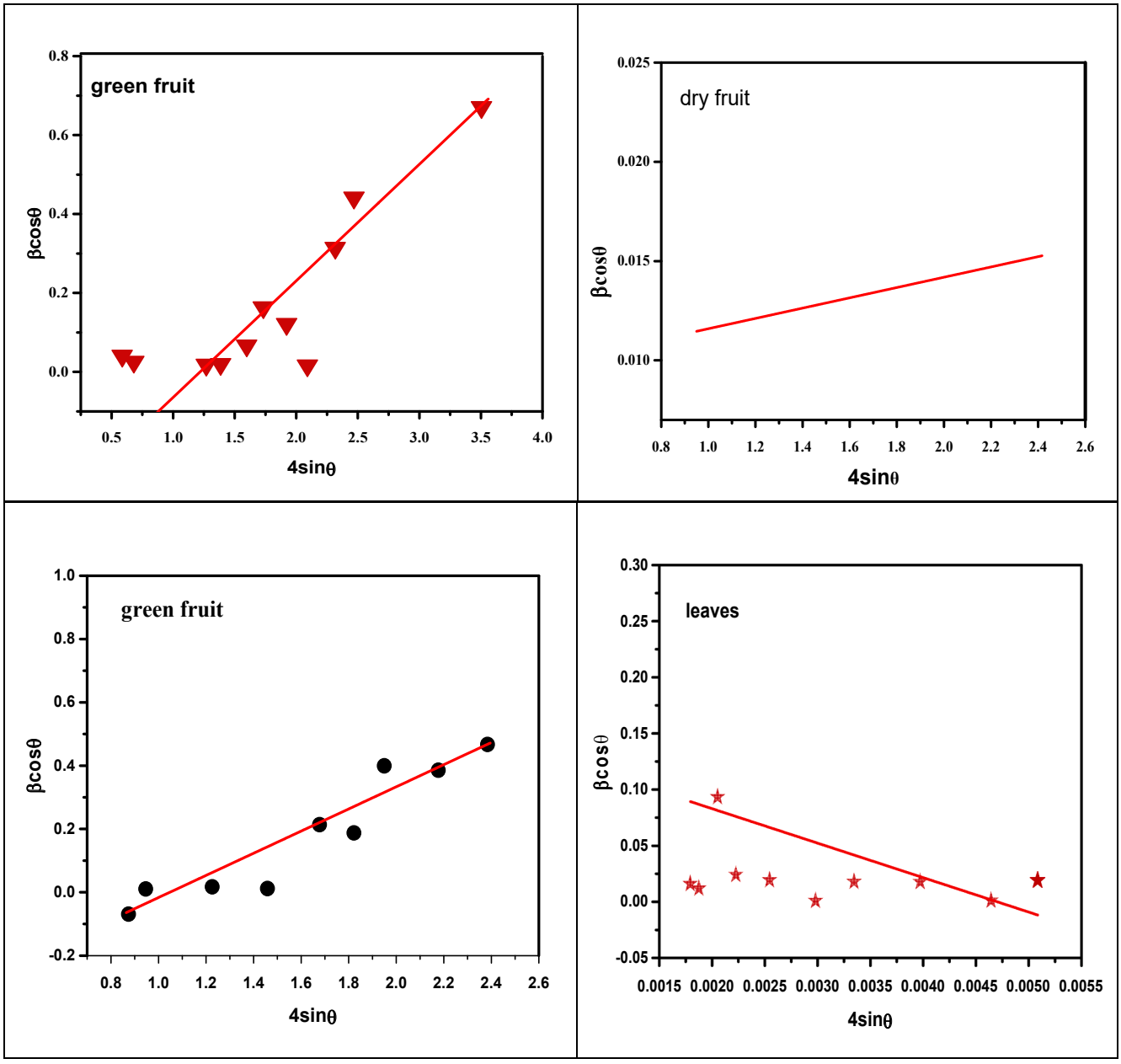

Fig. 6. WH-plot of FeO NPs.

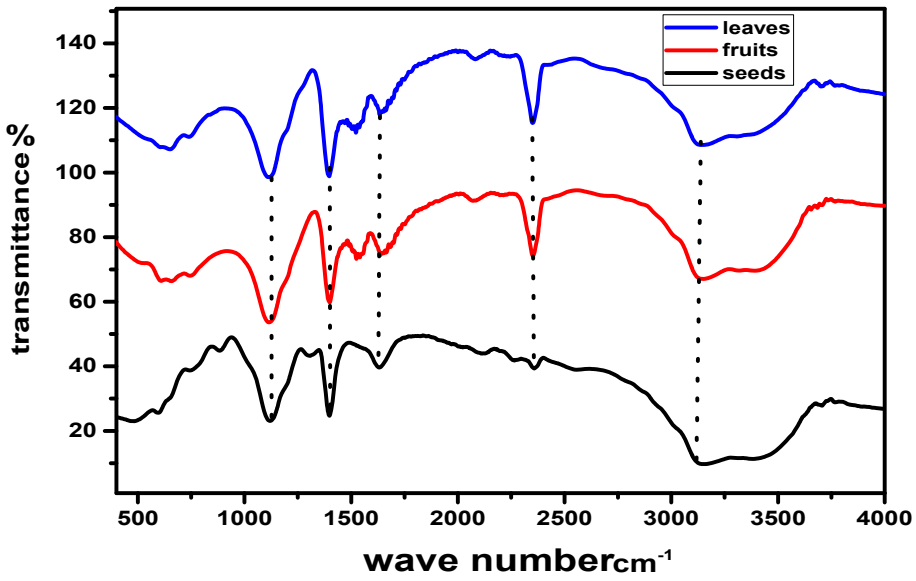

Fig. 7. FTIR spectrum of FeO-NPs.

are due to the phenolic components' **OH stretching** vibrations and this **–OH bond** from the aqueous phase. The **C = O stretching** vibration is represented by the band 1640–1740 cm^{-1} that denotes the phytochemicals exist in the plant extract. The **C–C stretch** of aromatic components and the **C–N stretch** of aromatic amines because aromatic hydrocarbons have a secondary amine, contribute bands at 1393 cm^{-1} region and 1118 cm^{-1} respectively. The **C–H bend** of alkenes is responsible for the bands in the nanoparticle spectrum ranging from 600 cm^{-1} to 1000 cm^{-1}. The engagement of the extract's functional groups in the formation of nanoparticles is responsible for the difference in bands (Sandhya and Kalaiselvam, 2020).

4.3. UV–Visible

The optical parameters (absorbance) of synthesized nano-particles of iron oxide were measured at room temperature, the absorbance spectra versus wavelength curve of all samples around 300 and 800 nm presented in Fig. 8. The UV–visible specimen was prepared by taking amount 0.05 g of samples and by dissolving every specimen in 10 mL of DMF solution. The UV–visible absorbance spectrum of iron oxide nanoparticles was measured for investigating the optical characteristics such as band gap energy. It has been observed the FeO NPs showed the broad absorption spectra from 340 to 380 nm throughout the spectral range this is attributable to the light being absorbed and scattered by nanoparticles (Devi et al., 2018). While absorbance band of seeds observed at 400–520 nm wavelength range. The band gap energy was examined by using Tauc relation, (Anjum et al., 2012)(See Fig. 9).

$$\alpha hv = A(hv - Eg)^{n} \tag{4.13}$$

Where (Eg) is the band gap energy, A is constant which doesn't depend on hv and n (1, 1/2) for direct and indirect band gap.

Indirect and direct band gap energy was examined by visualizing $(h\nu\alpha)^{1/2}$ and $(h\nu\alpha)^{2}$ as a function of photon energy ($h\nu$), respectively. In an indirect band gap, a photon cannot be emitted instantly because the

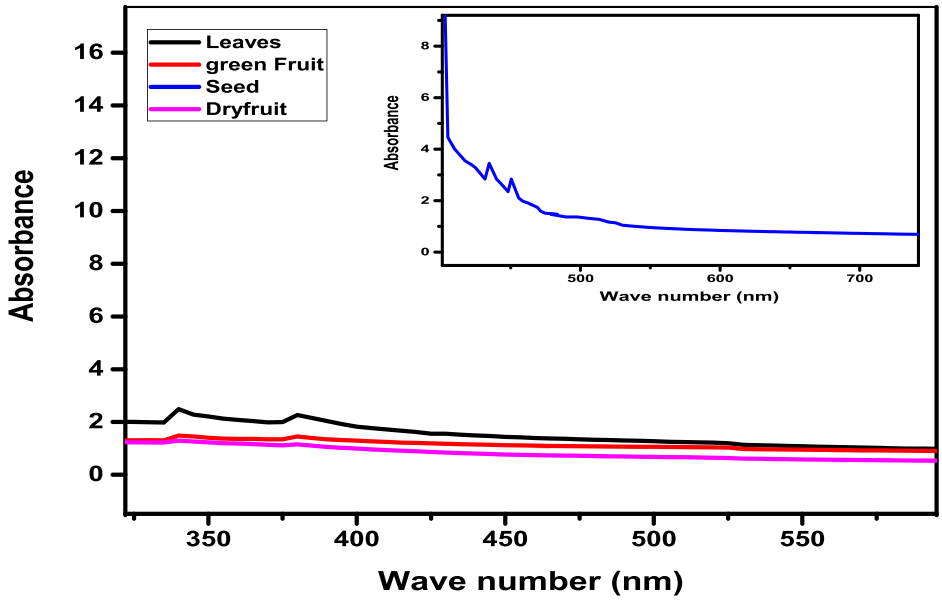

Fig. 8. UV–Visible absorption spectra of FeO NPs.

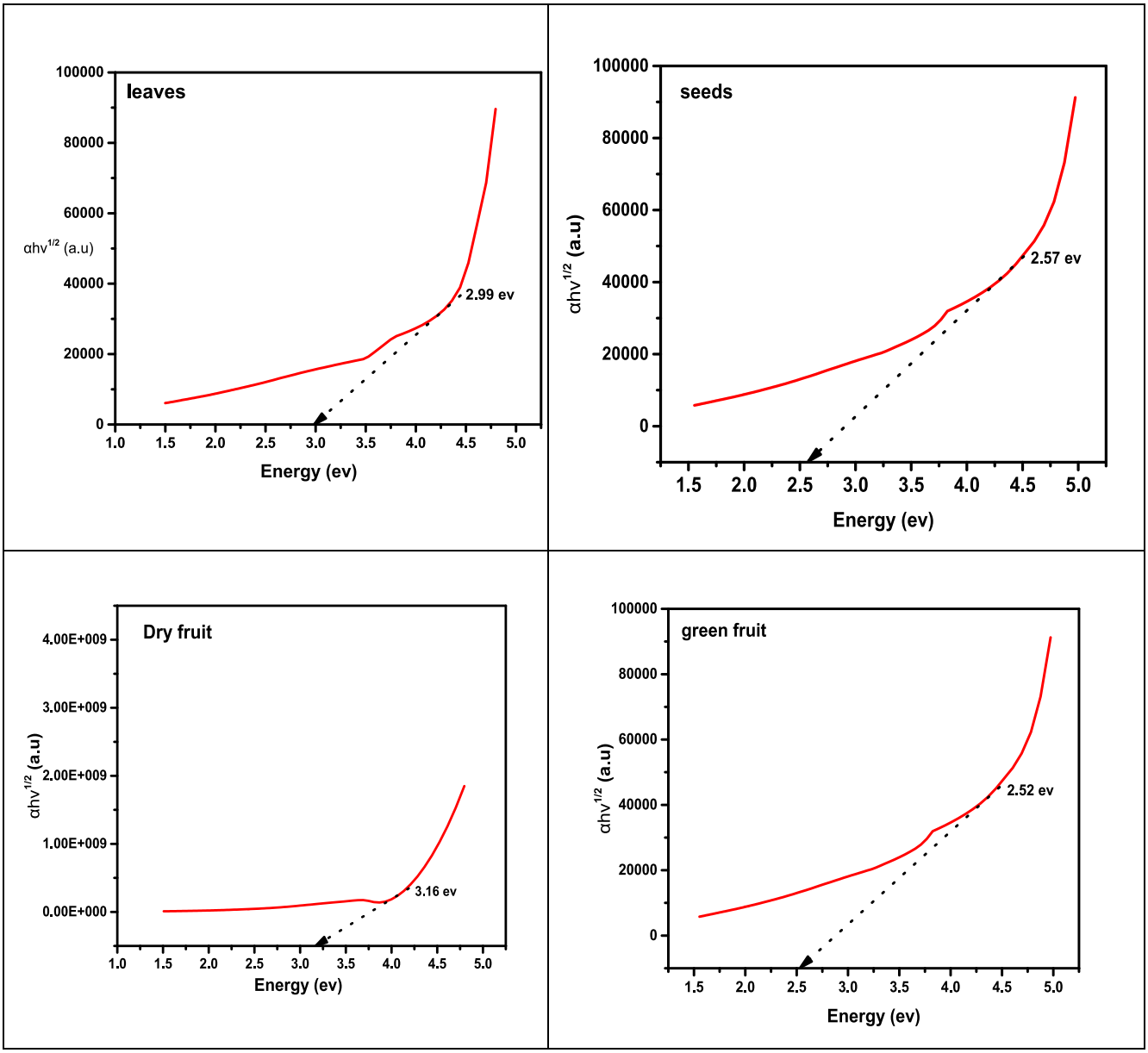

Fig. 9. Indirect band gap of FeO NPs.

electron may shift to an intermediate state and pass its momentum towards the lattice structure. The band energies of dry fruit, seeds, leaves and green fruit are 3.16 eV, 2.57 eV, 2.99 eV and 2.52 eV respectively.

The significant changes in the conduction band's density occur when material is decreased from bulk to nanoscale. As particle size is reduced, the energy band gap and the space between electrical levels increase. Consequently, the electron's hole pair increased close to one another and the fact that their Columbic interaction can no longer be ignored, the kinetic energy of the molecules as a whole has increased (Moscoso-Londoño et al., 2017). In addition, a higher band gap caused it takes more energy to drive an electron from the valance band to the conduction band, higher frequency, shorter wavelength is absorbed. It has been observed the optical band gap energy also decreased as crystallite size increases, as a consequence the decreasing band gap makes samples conductive because the distance between the valance and conductive band decreases.

4.4. SEM analysis

The morphological screening of fabricated iron-oxide NPs has significant role in terms of structure and size were studied by SEM. The morphology of fabricated FeO NPs presented in Fig. 10 (a-c). The obtaining SEM images shows the formation of Fe-O NPs at 300kx magnification level. The figure (a-c) exhibits SEM images with diameter distribution for dry fruit, leaves and green fruit and the grain size is **3.9034x10^{3}nm, 25.15984x 10^{3}nm** and **3.5532x 10^{3}nm** respectively. **Figure (a)** illustrates that the nature of the manufactured nanoparticles are not uniform. The vast agglomerated cluster was discovered as a result of accumulation of tiny building block of biological active reducing agent of plant extract. This may also be related to the plant extract's poor tendency for agglomeration of iron oxide-based nanoparticles caused by magnetic interaction. **Figure (b and c)** exhibits the formation of cube shaped FeO-NPs. This slightest cubic shaped NPs has induced by plant enzymes.

SEM revealed that nanoparticles of iron oxides are irregular in shape. The high surface charge on iron oxide nanoparticles and magnetic

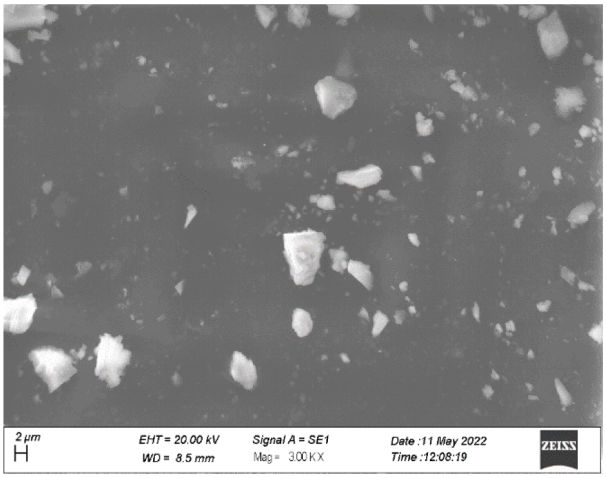

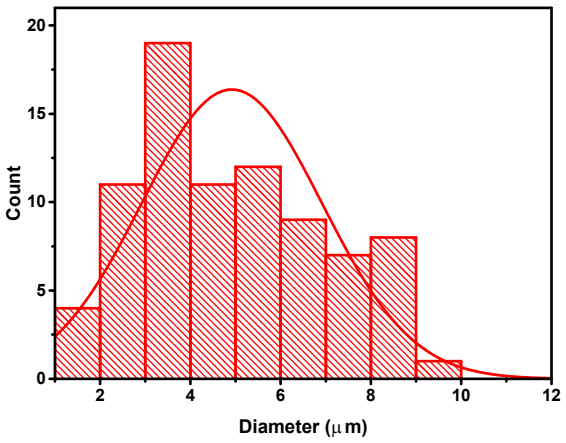

(a) Green fruit

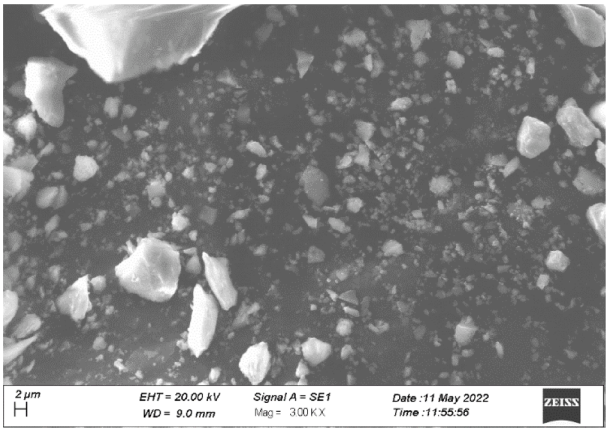

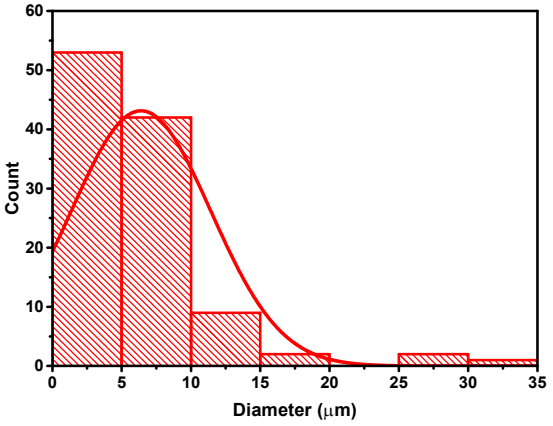

(b) Leaves

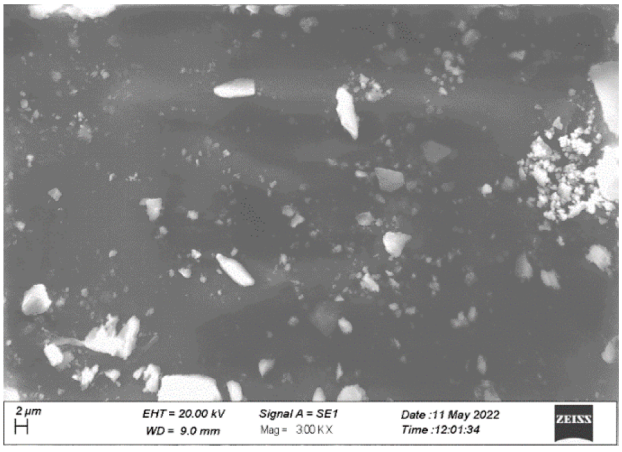

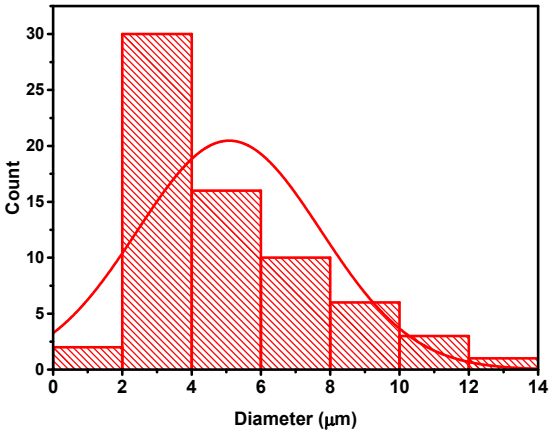

(c) Dry fruit

Fig. 10. SEM images of synthesized FeO NPs.

interactions may be the cause of this, as the FeO nanoparticles are well consistent with even the slightest agglomeration.

The edx analysis are presented in Fig. 11(a,b,c). From the result it can be seen that the quantity of Au, is detected due to sputtring of gold on sample while the Fe and O will confirm the formation of Fe3O4. The presence of tape is captured in the form of C and Cl is detected due to FeCl3 doping during the synthesis process. The weight and atomic % is presented in Table 3.

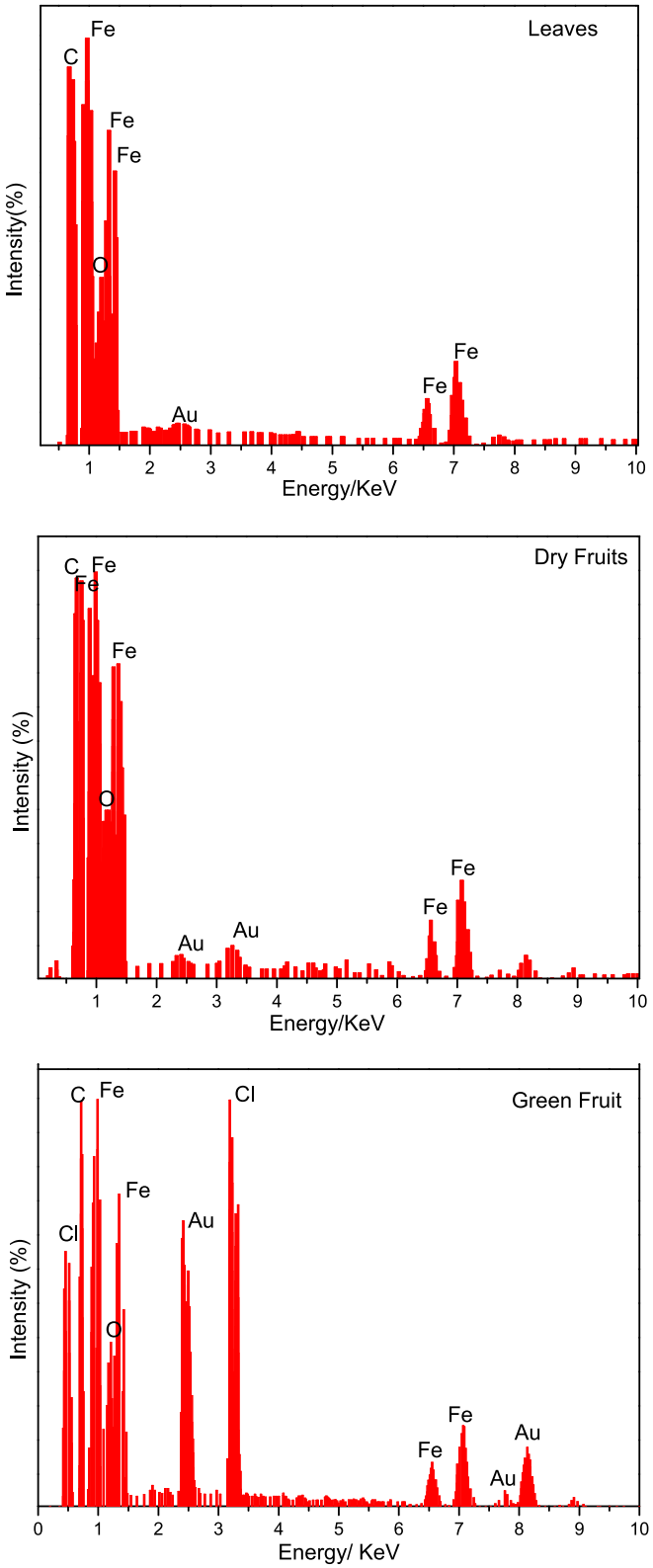

Fig. 11. (a,b,c): the Edx spectrum of leaves, dry and green fruit against energy.

4.5. XPS analysis

The XPS spectrum of iron oxide nanoparticles produced through green fruit is presented in Fig. 12. From the results, it can be seen that the overview of green fruit nano particles exhibits the presence of carbon, oxygen, iron, nitrogen and chlorine. While on the other hand, in C1s the peak of C–C, C-O-C and O = C is detected at 284.9, 286.6 and 288.3 eV respectively. The Fig. 12 c shows the valuable information about deconvolution of O1s which provides the information of chemical state of oxygen in prepared nanoparticles (Win et al., 2021). The peak of lattice oxygen (O in Fe-O–H) is observed at 529.85 eV which is well match other method of green synthesis of iron oxide nano particles (Win et al., 2021) While the peak at 531 eV representing the Fe-O. These binding energy peaks are observed because of Fe and oxygen based functional groups (Win et al., 2021). From Fig. 12d the deconvolated peaks are observed because of pyrrolic nitrogen and N-C bonding which confirms the formation of iron oxide nanoparticles.

4.6. Antibacterial activity

On Luria Bertani Agar (LBA) media, Avicennia marina leaves samples were inoculated. After incubation for 24 h at 25 °C, bacterial growth was clearly visible. The bacterial colonies has been purified by streaking method in separate plates. Pseudomonas syringae and Bacillus species has been identified.

Iron oxide nanoparticles were synthesized using Avicennia marina leaves extract and their antibacterial activity has been estimated against gram negative and gram-positive strains. Iron oxide nanoparticle from 2 g leaf powder sample and 4 g leaf powder sample has been used against Escherichia coli to check inhibition zones. The diffusion strategy has been effectively used (Chennimalai et al., 2021).

Inhibition zone of Xanthomonas campestris pv vesicatoria strain with iron oxide nanoparticles of 2 g sample was 2.5 cm or 25 mm Fig. 13. The inhibition zone of Erwinia spp strain with iron oxide nanoparticles of 2 g sample was 3.5 cm or 35 mm. The inhibition zone of E. coli strain with iron oxide nanoparticles of 2 g sample was 4.5 cm or 45 mm.

5. Conclusion

Iron oxide nanoparticles have been successfully synthesized by green synthesis technique. This environmentally friendly effort is contribute to the formation of materials that are less hazardous, compatible with electrical and electronic industries, and of higher quality for use in daily life. A green process has been used to create nanoparticles of iron oxide via Avicennia marina (leaves, fruit and seed) extract. Green route is very eco-friendly, inexpensive and simple fabrication method. XRD, FT-IR, SEM, and UV–Visible were utilized to analyze the synthesized FeO NPs. The structural characterization results confirmed the fabrication of highly crystalline iron oxide nanoparticles of Avicennia marina's (dry fruit, seeds leaves and green fruit) with crystallite size(7.1335 nm, 9.295 nm, 9.680 nm, 10.128 nm) respectively. The XRD revealed the single phase cubic structure. The FT-IR spectra stated the surface

Table 3
The concentration of weight and atomic %.

Elemental Analysis:						
	Weight %	Atomic %	Weight %	Atomic %	Weight %	Atomic %
	Leaves		Dry fruits		Green fruits	
Fe	1.20	28.82	1.29	27.83	1.32	29.76
O	0.792	71.18	0.73	72.17	0.68	0.65
Total	1.992		2.02		2.00	

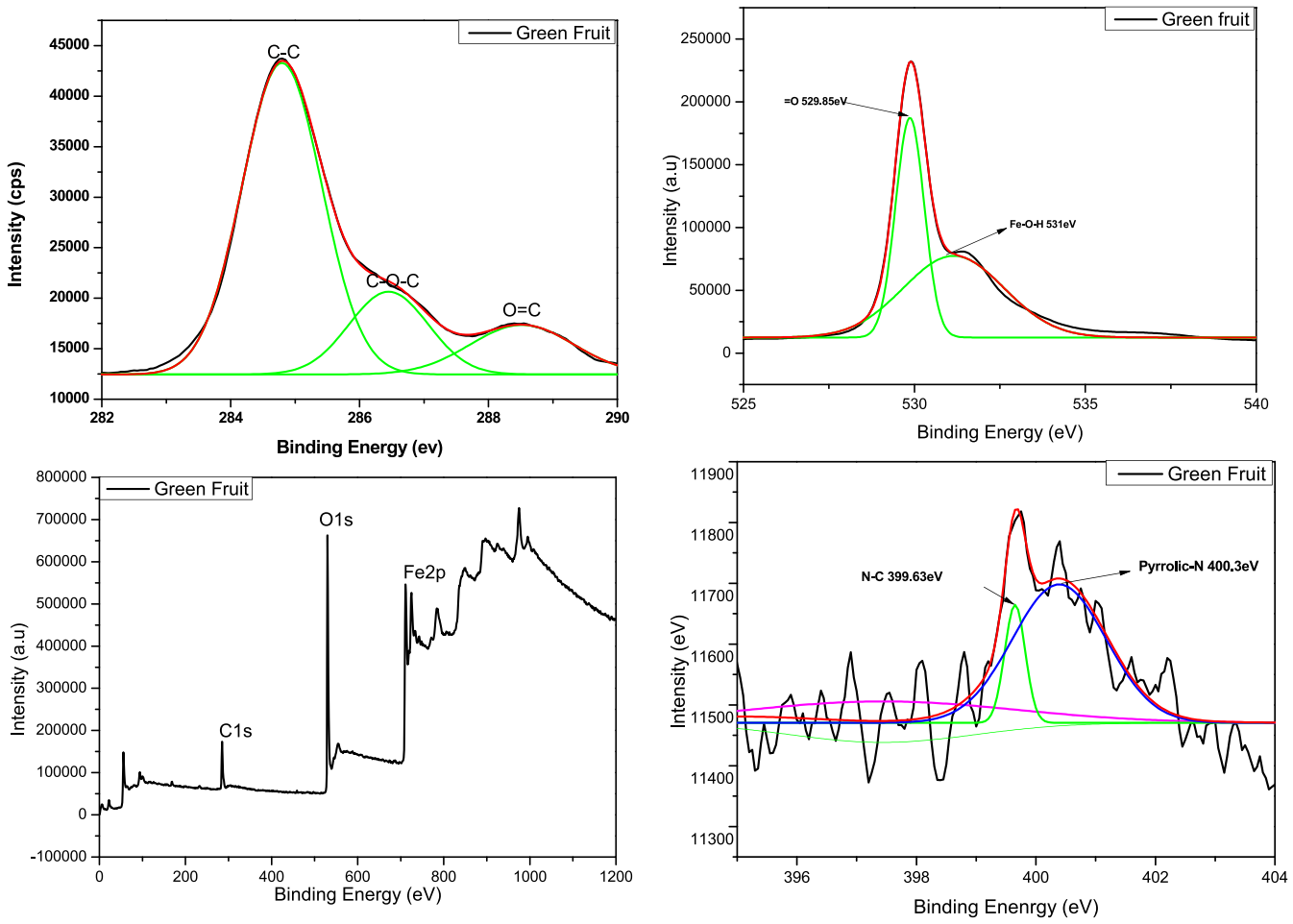

Fig. 12. (a,b,c,d): XPS analysis (C1s, O1s, N1s, and general view) of green fruit.

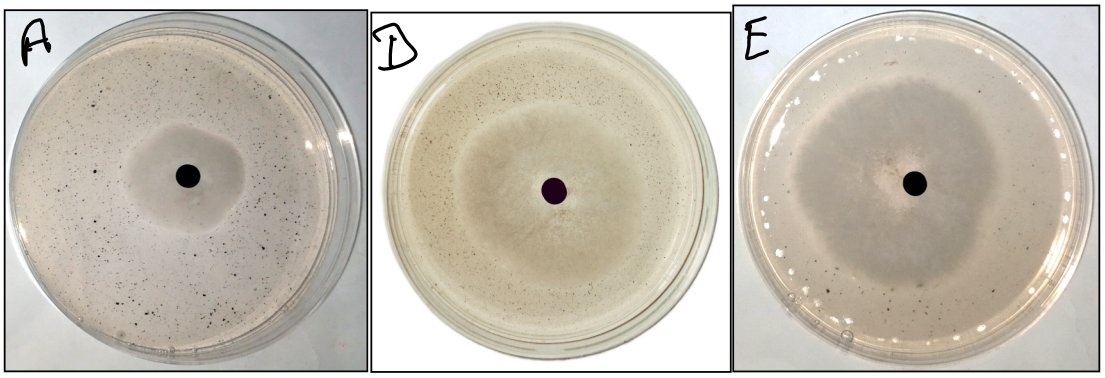

Fig. 13. Antibacterial activity of iron oxide nanoparticles against xanthomonas campestris pv vesicatoria (a), erwinia spp (d), escherichia coli (e).

functionalization of fabricated iron oxide nanoparticles. FT-IR measurement revealed the attachment of compound, functional groups found in phenolic component which are due to O–H stretching that can be helpful in the development of metallic nanoparticles. The band gap energies decreasing as crystallite size increases, according to UV visible results band gap energies of dry fruit, seeds, leaves and green fruit are 3.16ev, 2.57ev, 2.99ev and 2.52ev respectively. The morphological screening of fabricated iron-oxide NPs visualized by SEM, this revealed that the nanoparticles are slightest cubical and irregular in shape. The calculated grain size of the dry fruit, leaves and green fruit are $3.9034x10^3$nm, $25.15984x\ 10^3$nm and $3.5532x\ 10^3$nm respectively. The fabricated nanoparticles has been examined for antimicrobial properties against Xanthomonas campestris pv vesicatoria, Erwinia spp, Escherichia coli bacteria's. These nano particles were utilized for antimicrobial activity because of their less toxicity, high stability and biocompatibilities. Hence it could be concluded that these FeO NPs can be used as antibacterial agent and iron oxide nanoparticles minimize on bacterial colony. Furthermore it might be concluded that this environmentally friendly process of producing iron oxide nanoparticles is an effective way to create highly biocompatible nanoparticles with improved therapeutic benefits. More research proceed to explore iron oxide nanoparticles' outcomes with drugs frequently used for these bacterium.

Declaration of competing interest

The authors declare that they have no known competing financial interests or personal relationships that could have appeared to influence the work reported in this paper.

Acknowledgement

The authors extend their appreciation to the Deanship of scientific research at king Khalid University for funding this work through research group under grant number R.G.P-2/270/44. We are grateful to Silesian University of Technology, Poland, and Lahore College for Women University, Lahore, Pakistan for their support of research activities.

References

A, R and west, Solid State Chemistry and its Applications, 2007.

Ahila, K., Vasanthy, M., Thamaraiselvi, C., 2018. Green synthesis of magnetic iron nanoparticle using Moringa oleifera Lam seeds and its application in textile effluent treatment. Util. Manage. Bioresour. Springer 315–324.

Amutha, T., Rameshbabu, M., Sasi Florence, S., Se, N., 2019. "Studies on structural and optical properties of pure and transition metals (Ni, Fe and co-doped Ni–Fe) doped tin oxide (SnO 2) nanoparticles for anti-microbial. Res. Chem. Intermed. 45, 1929–1941.

Anjum, S., Rafique, M.S., Khaleeq-ur Rahman, M., 2012. Investigation of induced parallel magnetic anisotropy at low deposition temperature in Ba-hexaferrites thin films. J. Magn. Magn. Mater. 324 (5), 711–716.

A, Attarad, Z, Hira, Z, Muhammad, H, U and İhsan, Synthesis, characterization, applications, and challenges of iron oxide nanoparticles Nanotechnol. Sci., 2016, pp. pp. 49-67.

Awwad, A.M., Salem, N.M., Aqarbeh, M.M., Abdulaziz, F.M., 2020. Greensynthesis, characterization of silver sulfide nanoparticlesand antibacterial activity evaluation. Chem. Int. 42–48.

C. B., Element of X-ray diffraction, AddisonWesley reading. MA Google Scholar, 1978.

Chennimalai and M., T. S. Senthil, Misook Kang, and N. Senthilkum, ""A novel green-mediated approach of 3-D hierarchical-like ZnO@ Ag, ZnO@ Au and ZnO@ Ag@ Au NCs prepared via Opuntia ficus indica fruits extract for enhancement of biological activities," *Applied Physics A 127, no. 8,* p. 611, 2021.

Darroudi, M.e.a., 2014. Superparamagnetic iron oxide nanoparticles (SPIONs): Green preparation, characterization and their cytotoxicity effects. Ceram. Int. 14641–14645.

DeviHS, BodaMA, ShahMA and Parveen S and Wani , Green synthesis of iron oxide nanoparticles using Platanus orientalis leaf, 2018, pp. 38-45.

L. K. O. R. T. M. R. F. A. D. M. Gholami, Green facile synthesis of low-toxic superparamagnetic iron oxide, 06/01/2018.

Igwe, O.U., Nwamezie, F., 2018. Green synthesis of iron nanoparticlesusing flower extract of Piliostigma thonningii and antibacterialactivity evaluation. Chem. Int. 4, 60–66.

P. H. S. S. A. F. A. K. F. J.-A. K. &. D. F. Imanipour, Imanipour, P., Hasani, S., Seifoddini, A. and Farnia,, The possibility of vanadium substitution on Co lattice sites in CoFe2O4 synthesized by sol–gel autocombustion method. Journal of Sol-Gel S, 2020.

Jayapriya and M. Arulmozhi, E. Nandhakumar, N. Senthilkumar, and, ""Green synthesis of silver nanoparticles using Piper longum catkin extract irradiated by sunlight: antibacterial and catalytic activity.," *Research on Chemical Intermediates 45.,* pp. 3617-3631, (2019).

S. a. Kanagasubbulakshmi and K. Kadirvelu., "Green synthesis of iron oxide nanoparticles using Lagenaria siceraria and evaluation of its antimicrobial activity.," " *Defence Life Science Journal 2, no. 4,* pp. 422-427., (2017).

Karpagavinayagam, "Green synthesis of iron oxide nanoparticles using Avicennia marina flower extract.," vol. Vacuum 160 , pp. 286-292, (2019).

Krishnan, B.R., Ramesh, A.S.S.K.M., Selvakumar, M., 2020. A facile green approach of cone-like ZnO NSs synthesized via jatropha gossypifolia leaves extract for photocatalytic and biological activity. J. Inorg. Organomet. Polym Mater. 30, 4441–4451.

Laurent, Forge, S., Robic, Roch and Port, Magnetic iron oxide nanoparticles: synthesis, stabilization, vectorization, physicochemical characterizations, and biological applications. Chem., vol. Rev. 108, 2008, p. 2064–2110.

Moscoso-Londoño, Tancredi, Muraca, Zélis, P. M., Coral, D. and van Raap & Socolovsky, Different approaches to analyze the dipolar interaction effects on diluted and concentrated granular superparamagnetic systems. Journal of Magnetism and Magnetic Materials, 428, 2017, pp. 105-118.

L. Nadi, Modern Trend Phys. Res, 2013.

Nguyen, X.P., 2012. Tran, pham, N and H, iron oxide-based conjugates for cancer theragnostics. Adv. Nat. Sci. Nanosci. Nanotechnol. 3, 033001.

parveen, S., Misra, R., Sahoo, S.K., 2012. Nanoparticles: a boon to drug delivery, therapeutics, diagnostics and imaging. Nanomed. Nanotechnol. Biol. Med. 8, 147–166.

R, M, Patil, N, D, Thorat, P, B, Shete and Bedge, Bohara Comprehensive cytotoxicity studies of superparamagnetic iron oxide nanoparticles, 2018, pp. PP 63-72.

Rajivgandhi,, G, Franck, Q, Muthusamy and Ji- Mi, Muthuchamy, M., Muneeswaran, T., Biologically synthesized copper and zinc oxide nanoparticles for important biomolecules detection and antimicrobial applications. Mater. Today Commun. 22, 100, 2020.

RamalinVaikundamoorthy and S. S. Pandurangan Dhinesh, ""Green fabrication of iron oxide nanoparticles using grey mangrove Avicennia marina for antibiofilm activity and in vitro toxicity.," " *Surfaces and Interfaces,* pp. 70-77, 2019.

Remya, V.R., Abitha, V.K., Rajput, P.S., Rane, A.V., Dutta, A., 2017. Silvernanoparticles green synthesis: a mini review. Chem. Int. 165–171.

Sandhya, J., & Kalaiselvam and S., Biogenic synthesis of magnetic iron oxide nanoparticles using inedible borassus flabellifer seed coat: characterization, antimicrobial, antioxidant activity and in vitro cytotoxicity analysis. Materials Research Express, 7(1), 015045, 2020.

S.K. Sen, T.C. Paul, S. Dutta, M.N. Hossain and M.N.H, optical properties analysis of Ag-doped h-MoO3 nanorods synthesized via hydrothermal method, J. Mater. Sci. Mater. Electron. 31, 2020, p. 1768–1786.

Tartaj, P, Morales, González-Carreño, S and V, Advances in magnetic nanoparticles for biotechnology applications J. Magn. Magn. Mater, vol. 290–291, 2005, pp. pp. 28-34.

Teja, A.S, Koh, P and Y, Synthesis, properties, and applications of magnetic iron oxide nanoparticles. In: Progress in Crystal Growth and Characterization of Materials, vol. vol. 55, 2009/03/01/2009, p. pp. 22–45.

Toropov, N, Vartanyan and T, Noble Metal Nanoparticles: Synthesis and Optical Properties, 2019.

Williamson, G.K., Hall, W.H., 1953. X-ray line Broa dening from filed aluminium and Wolfram. Acta Metall.

Win, T.T., Khan, S., Bo, B., et al., 2021. Green synthesis and characterization of Fe3O4 nanoparticles using Chlorella-K01 extract for potential enhancement of plant growth stimulating and antifungal activity. Sci Rep 11, 21996. https://doi.org/10.1038/s41598-021-01538-2.

Zeeshan, T., Anjum, S., Waseem, S., Majid, F., 2021. A, Influence of zinc substitution on structural, elastic, magnetic and optical properties of cobalt chromium ferrites. Mater. Sci.-Pol. 39 (1), 139–151.